

## Alignment of Polarization against an Electric Field in van der Waals Ferroelectrics

Sabine M. Neumayer<sup>1</sup>,<sup>✉</sup> Lei Tao,<sup>2,3</sup> Andrew O'Hara<sup>2</sup>,<sup>✉</sup> John Brehm,<sup>2</sup> Mengwei Si<sup>4,5</sup>,<sup>✉</sup> Pai-Ying Liao<sup>4,5</sup>,<sup>✉</sup> Tianli Feng,<sup>2,3</sup> Sergei V. Kalinin,<sup>1</sup> Peide D. Ye,<sup>4,5</sup> Sokrates T. Pantelides<sup>2,6</sup>,<sup>†</sup> Petro Maksymovych,<sup>1,‡</sup> and Nina Balke<sup>1,\*</sup>

<sup>1</sup>Center for Nanophase Materials Sciences, Oak Ridge National Laboratory, Oak Ridge, Tennessee, USA

<sup>2</sup>Department of Physics and Astronomy, Vanderbilt University, Nashville, Tennessee 37235, USA

<sup>3</sup>University of Chinese Academy of Sciences & Institute of Physics, Chinese Academy of Sciences, Beijing 100190, China

<sup>4</sup>School of Electrical and Computer Engineering, Purdue University, West Lafayette, Indiana 47907, USA

<sup>5</sup>Birck Nanotechnology Center, Purdue University, West Lafayette, Indiana 47907, USA

<sup>6</sup>Department of Electrical Engineering and Computer Science, Vanderbilt University, Nashville, Tennessee 37235, USA



(Received 22 January 2020; revised manuscript received 27 May 2020; accepted 29 May 2020; published 26 June 2020)

Polarization in ferroelectrics can be switched in the direction of an applied electric field by dipole reorientation, enabling numerous applications and fundamental phenomena. Here, we demonstrate that, in the van der Waals (vdW) layered ferroelectric  $\text{CuInP}_2\text{S}_6$ , a unique mechanism exists where polarization aligns against the direction of the applied electric field, seemingly in violation of the fundamental properties of a dipolar solid. The mechanism is the result of the electric field driving the Cu atoms unidirectionally across the vdW gaps, which is distinctively different from dipole reorientation. The crossing of Cu atoms is the fundamental process of ionic conductivity, yet it is compatible with the existence of polarization. These phenomena are confirmed by nanoscale imaging and spectroscopy of ferroelectric capacitors, coupled with dynamic density-functional-theory simulations. The symbiotic relationship of ferroelectric and ionic phenomena enables alternative approaches to control polarization and necessitates a change in perspective on nucleation, domain-wall dynamics, and other ferroelectric and electromechanical characteristics in material systems where ionic and ferroelectric phenomena manifest.

DOI: [10.1103/PhysRevApplied.13.064063](https://doi.org/10.1103/PhysRevApplied.13.064063)

### I. INTRODUCTION

In a canonical ferroelectric, spontaneous symmetry breaking below the Curie temperature creates at least two equivalent atomic configurations with opposite orientations of spontaneous polarization. An external electric field preferentially lowers the energy of one of these configurations, switching polarization in the direction of the field. In some ferroelectrics, applied electric fields can also induce ionic transport, which is believed to be incompatible with the ferroelectric state or, at least, is a limiting factor for ferroelectric switching, if both properties are mediated by the same ionic species [1,2]. This notion is based on the fact that ionic conductivity is promoted by, and can itself generate, atomic disorder, whereas the ferroelectric state is ordered [3–5]. Indeed, ionic processes, so far, are mainly discussed in the extrinsic context of defects and interfaces,

such as ionic screening of spontaneous polarization [6–8] and leakage conductivity [9]. In ferroelectric ion conductors, such as  $\text{Ag}_{26}\text{I}_{18}\text{W}_4\text{O}_{16}$  [10] and  $\text{CsH}_2\text{PO}_4$  [11], both properties are typically discussed in different temperature ranges, but it has been proposed by Scott that adequately large voltages may enable a transition from ferroelectric switching to ion conduction [12].

Layered ferroelectric  $\text{CuInP}_2\text{S}_6$  exhibits both ferroelectricity [13–16] and ionic conductivity [17,18] at temperatures below the Curie temperature, providing an excellent platform where possible cooperative effects of both properties can be explored. The van der Waals (vdW) crystals comprise a  $\text{P}_2\text{S}_6$  anion sublattice [13,19] and a cation Cu sublattice with remarkably large, Å-scale spontaneous polar displacements, including a recently discovered high-polarization phase, with even larger displacements into the vdW gap [20,21]. The presence of two interconnected polar phases results in an unusual quadruple-well potential for Cu displacements [21]. The quadruple well has a very small energy barrier between the low- and high-polarization phases, but is tunable by strain, which

\*balken@ornl.gov

†pantelides@vanderbilt.edu

‡maksymovychp@ornl.gov

can stabilize either of the two phases. The quadruple well also enables a range of other unique properties, including a large negative electrostriction [20–22]. It is still unknown if there is an underlying connection between ionic conductivity and ferroelectricity.

Here, we report a fundamentally distinct physical mechanism for controlling the polarization states in  $\text{CuInP}_2\text{S}_6$ , enabling polarization to be aligned against the direction of the electric field. This feature is not caused by dipole reorientation, as in conventional ferroelectric switching, but can be understood once Cu displacements across the vdW gaps are considered. To elucidate the complex ferroelectric characteristics of  $\text{CuInP}_2\text{S}_6$ , we combine piezoresponse force microscopy (PFM) measurements on capacitor structures incorporating  $\text{CuInP}_2\text{S}_6$  as the active dielectric with density-functional-theory (DFT) calculations and quantum-molecular-dynamics (QMD) simulations of field-driven Cu displacements. By using voltage pulses of different durations, PFM measurements track Cu displacements through successive polarization states, which are identified by comparing measured and calculated piezoelectric coefficients. The observed polarization alignment against the electric field can be explained by moving Cu ions across the vdW gaps, which is also the fundamental step for ionic conductivity. DFT calculations and QMD simulations indicate that this mechanism is facilitated if excess Cu atoms or Cu vacancies are present in the lattice. This mechanism enables alternative approaches to control polarization, for instance, by sequential transitions among all four polarization states with electric fields of the same direction, which is impossible in a conventional dipolar solid. Moreover, the nature of this mechanism necessitates a different outlook on the physics of domain nucleation and domain-wall dynamics in the presence of ionic motion.

## II. METHODS

### A. Experiments

$\text{CuInP}_2\text{S}_6$  crystals are grown through a solid-state reaction. Powders of the four elements with the same stoichiometric ratio are mixed and placed in an ampoule and annealed under vacuum at 600 °C for 2 weeks.  $\text{CuInP}_2\text{S}_6$  flakes are transferred to the  $\text{Ni}(20\text{ nm})/\text{SiO}_2(90\text{ nm})/p + \text{Si}$  substrate by Scotch tape-based mechanical exfoliation. The top electrode, of 20 nm nickel, is fabricated using an electron-beam lithography, electron-beam evaporation, and lift-off process. The detailed device fabrication process can be found in Si *et al.* [23].

Polarization switching is studied by single  $V_{\text{dc}}$  pulse switching. The local evolution of polarization states is tracked on a  $\text{Ni}/\text{CuInP}_2\text{S}_6/\text{Ni}$  capacitor structure upon varying the duration of  $-6\text{ V}$  pulses in 10 steps between 100 ms and 1 s applied via an atomic-force-microscope probe placed at the center of the electrode. Before and

between these  $-6\text{ V}$  pulses, a reset pulse of  $+6\text{ V}$  is applied for 2 s. Switching experiments are conducted on a Bruker Icon atomic force microscope in an Ar-filled glove box. A Nanosensors PPP-EFM tip with a nominal force constant of 2.8 N/m and resonance frequency of 75 kHz is used. To obtain quantitative  $d$  values, the sensitivity of the cantilever is calibrated using the force-distance method and instrumental phase offsets are taken into account. PFM imaging of the  $\text{CuInP}_2\text{S}_6$  surface through the Ni top electrode is performed in band-excitation mode, and the pulses applied to the middle of the top electrode are generated using a function generator (Stanford Research Systems, DS345).

### B. Theory

The DFT calculations and molecular dynamics simulations of copper paths are performed using the Vienna *ab initio* simulation package (VASP) [24] with core-valence electron interactions described via the projected augmented wave (PAW) method [25,26]. Wave functions are expanded in a plane-wave basis using a 400 eV energy cutoff. Exchange and correlation effects are described using the Perdew-Burke-Ernzerhof [27] generalized gradient approximation, including van der Waals corrections via Grimme’s DFT-D3 method with Becke-Johnson damping [28,29]. The process of a Cu atom jumping across the van der Waals gap is simulated using a structural model containing four layers of the  $\text{CuInP}_2\text{S}_6$  structure, with four formula units per layer and a vacuum separation layer of 25 Å. All atomic positions are relaxed until the forces are smaller than 0.02 V/Å. The energy barriers are calculated using the climbing-image nudged-elastic band (CI NEB) method [30,31]. An external electric field ( $-1.0\text{ V/Å}$ ) along the  $z$  direction is applied using the methods of Neugebauer and Scheffler [32] and Makov and Payne [33]. The Brillouin zone is sampled using only the  $\Gamma$  point.

For quantum-molecular-dynamics simulations, a canonical ( $NVT$ ) ensemble is employed [34,35], along with an external electric field ( $-1.0\text{ V/Å}$ ) along the  $z$  direction (the  $NVT$  ensemble is a good approximation to nonequilibrium simulations because maintaining a constant temperature is achieved by rescaling the velocities of all atoms, so that the Cu ions are still allowed to accelerate under the electric field.) The time interval between MD steps is 10 fs. The ferroelectric process from initialization to 70 ps is simulated at 250 K. From 75 to 150 ps, the temperature is increased to 500 K to speed up the simulation.

## III. RESULTS AND DISCUSSION

### A. Polarization switching

Owing to large polar displacements of the  $\text{Cu}^+$  ions and the recently discovered tunable quadruple potential well,

$\text{CuInP}_2\text{S}_6$  exhibits a unique polarization structure, comprising two polar phases (hereafter LP and HP, indicating low and high polarization of  $\sim 5$  and  $\sim 11 \mu\text{C}/\text{cm}^2$ , respectively), and, therefore, four distinct polarization states,  $\pm\text{LP}$  and  $\pm\text{HP}$  [21]. The structures of these states are shown in Fig. 1(a). In the present work, polarization switching is observed in Ni/ $\text{CuInP}_2\text{S}_6$ /Ni capacitors, by applying a sequence of voltage pulses to the top capacitor electrode and imaging the domain structure using PFM [Fig. 1(b)]. First, the capacitor is preconditioned with +6 V for 2 s, which orients the ferroelectric polarization pointing toward the bottom electrode (negatively). Subsequently, we apply negative pulses of  $-6$  V with increasing duration between 0.1 and 1 s, with the goal of observing the evolution of polarization during these time increments.

After each negative pulse, the remnant domain structure of  $\text{CuInP}_2\text{S}_6$  is imaged, and a reset pulse of +6 V is again applied for 2 s to reset the polarization to the original state. Overall, this procedure is similar to a first-order reversal curve that is commonly used to study ferroelectric and ferromagnetic material properties [36–40].

The changes in the measured piezoelectric coefficient,  $d$ , across the whole capacitor are visualized as a three-dimensional histogram of the effective piezoelectric coefficient,  $d$ , as extracted from PFM measurements for different negative-pulse durations [Fig. 1(b)]. At the same time, the  $d$  maps in Fig. 1(c) yield information on the spatial distribution of the electromechanical response. After preconditioning, the capacitor shows spatially uniform large positive  $d$  values centered around 50 pm/V. With

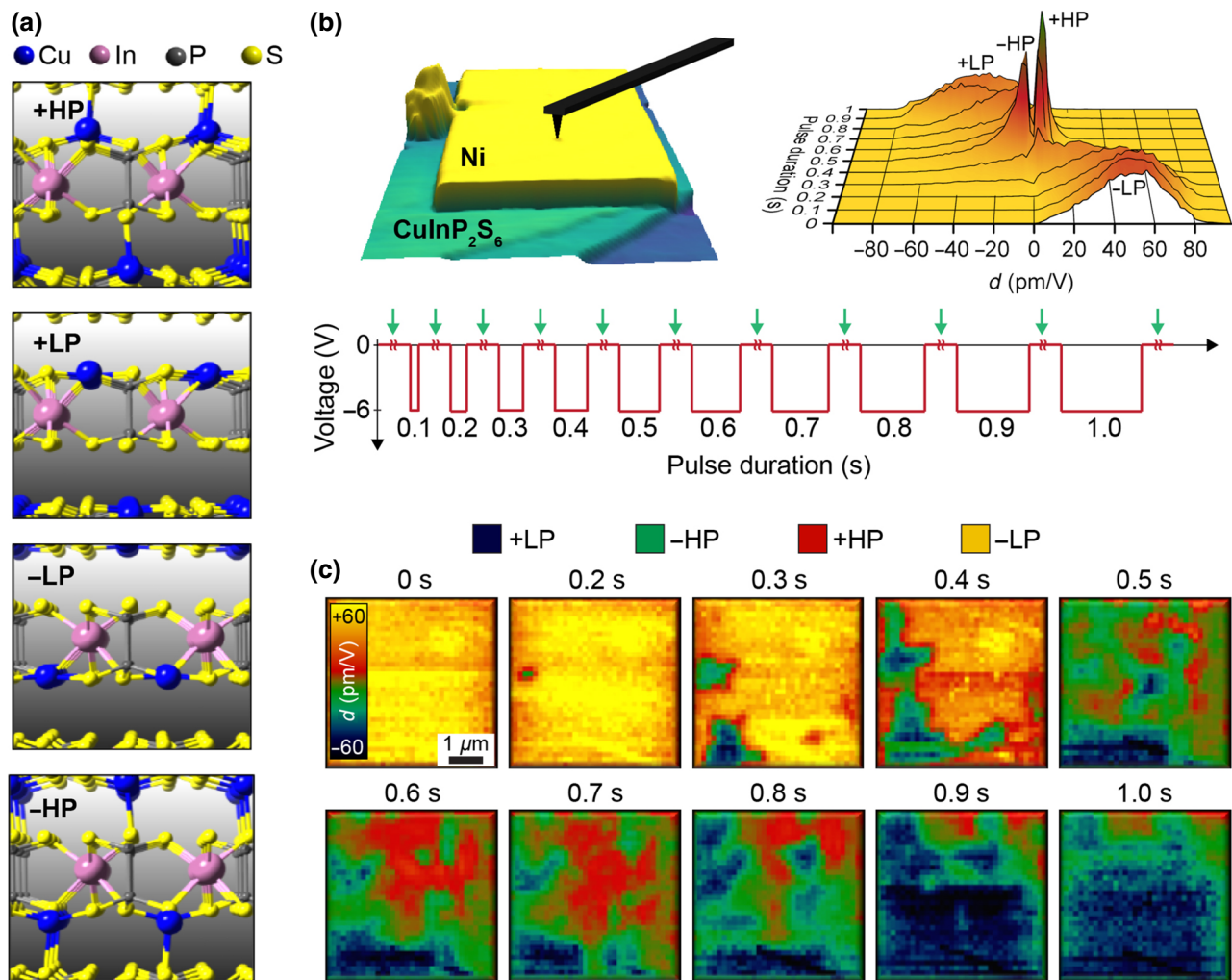


FIG. 1. Electromechanical response as a function of  $V_{\text{dc}}$  pulse duration. (a) Structural phases for each of the four polarization states in  $\text{CuInP}_2\text{S}_6$ : two upward-oriented polarization states (+HP and +LP) and two downward-oriented polarization states (-LP and -HP). (b) Three-dimensional topography image of Ni electrode on layered  $\text{CuInP}_2\text{S}_6$  and schematic depiction of the experimental setup. Sequence of applied voltage pulses; green arrows indicate when the PFM data are acquired. Three-dimensional histogram of measured  $d$  values as a function of pulse duration time. Distribution of counts is indicated by the height. (c) PFM maps of the Ni/ $\text{CuInP}_2\text{S}_6$ /Ni capacitor structure acquired after applying  $V_{\text{dc}}$  pulses, showing spatial variation in piezoresponse. Plot titles indicate duration of  $V_{\text{dc}}$  pulses; a 0.1 s pulse is omitted, as it does not show any differences from that of 0 s.

increasing negative-pulse duration (0.1–1 s), we observe the appearance of spatial heterogeneity and two very distinct low  $d$  values, at around  $\pm 5$  pm/V, and eventual transition to a relatively spatially uniform state with a piezoelectric constant of  $d \sim -40$  pm/V. Although the capacitor is repeatedly reset prior to each switching voltage pulse, the characteristic features in the PFM maps in Fig. 1(c) appear reproducibly, allowing the domain growth to be tracked. The spatial contrast of the electromechanical response [Fig. 1(c)] can be attributed to inhomogeneities in the Ni/CuInP<sub>2</sub>S<sub>6</sub> interface, which alters the local electric field distribution and can serve as domain nucleation centers [41,42].

The two polarization phases that are theoretically predicted and observed in CuInP<sub>2</sub>S<sub>6</sub> have distinct piezoelectric properties [21]. Strain-dependent DFT calculations show that the piezoelectric response is opposite in sign and varies in amplitude between the LP and HP phases, with piezoelectric constants,  $d_{33}$ , of  $-15.6$  pm/V for the LP and  $+2.5$  pm/V for the HP phases. Experimental values obtained by PFM on bare CuInP<sub>2</sub>S<sub>6</sub> surfaces match the theoretical values closely [21], while values measured through the top capacitor are higher and closer to those estimated from x-ray diffraction for single crystals [22]. The differences can be attributed to the capacitor thin-film geometry, resulting in partial clamping [43]. To compare the values consistently to theory, we therefore rely on ratios of low and high PFM response in both theory and experiment. The ratio of  $d$  for +HP and +LP is  $-6.24$  based on DFT values, and  $-6$  to  $-8.5$  measured on bare surfaces [21]. For the top capacitor, we observe similar average ratios of  $-8$  and  $-10$ , which enable us to identify and track the progression of HP and LP states through the measured piezoelectric response.

Based on the aforementioned ratios, we uniquely identify the four polarization states by the sign and amplitude of  $d$  as follows: about 50 pm/V corresponds to  $-LP$ , about

$-40$  pm/V to  $+LP$ , about 5 pm/V to  $+HP$ , and about  $-5$  pm/V to  $-HP$  [Figs. 1(b) and 1(c)]. Although Fig. 1 identifies all four polarization states participating in the switching process, their progression with pulse duration is rather complicated. As in the case of the PFM measurements on bare CuInP<sub>2</sub>S<sub>6</sub> surfaces [21], we observe four distinct polarization states, which suggests that the diffusion of Ni is not likely to play a substantial role.

## B. Switching paths

We visualize the evolution of the local response and polarization transitions as a Sankey diagram in Fig. 2. The diagram is constructed by plotting the number of pixels of each polarization state within individual PFM images along the  $y$  axis, while the  $x$  axis registers the voltage-pulse duration. The thickness of the lines indicates the number of pixels that undergo a certain polarization transition (heat maps of these results are shown in Fig. S1 within the Supplemental Material [44]). From the diagram, it is evident that only a small fraction of pixels transition in one step from  $-LP$  to  $+LP$  (yellow to blue transitions). Much more common are transitions from  $-LP$  to (sometimes multiple)  $+HP$  and  $-HP$  states before finally switching to  $+LP$ . The most extraordinary feature in the Sankey diagram is that some of the transitions appear to align the polarization against the electric field, e.g., positive polarization states transitioning to negative polarization states, such as from  $+HP$  to  $-HP$  (red to green transitions).

In the following, we analyze one of the intricate polarization switching pathways, as indicated by the white dotted line in Fig. 2. The progression of assigned polarization states along that trajectory is plotted in Fig. 3(a). During short pulse durations (0.1–0.7 s), the polarization changes from  $-LP$  to  $+LP$  and subsequently to  $+HP$ . Here, polarization aligns from negative to positive with the applied electric field, as expected for a dipolar solid. At a pulse

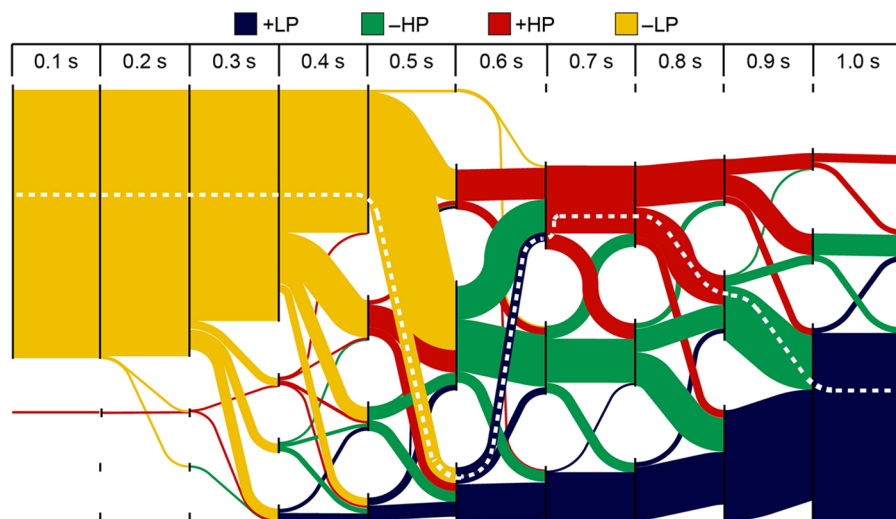


FIG. 2. Analysis of polarization-state transitions. Sankey diagram of polarization-state transitions dependent on voltage pulse calculated from transitions observed in the PFM maps shown in Fig. 1(c). Widths of the lines are proportional to the number of pixels that transition between two particular states for a given voltage step. White dashed line indicates the switching path discussed in detail in Fig. 3 and the text.

duration of 0.8 s, however, a transition from +HP to -HP states is observed, where the polarization vector aligns against the electric field direction, which contradicts the dipole reorientation mechanism in other ferroelectric materials. For 0.9 s pulses, the polarization transitions back to +LP, where the polarization again aligns with the electric field. When considering the structural phases of the polarization transition sequence [Fig. 3(b)], it becomes evident that the polarization pathway can be understood if we consider ionic conduction of the material, i.e., the fact that Cu can move in the direction of an applied electric field across layers and vdW gaps. If one specific Cu ion is tracked [red circle in Fig. 3(b)], the applied electric field moves it upwards, resulting in a transition of polarization states,

depending on where the Cu ion stops after the voltage pulse.

The unusual polarization sequence highlighted in Fig. 3(a) can now be understood by considering the trajectories and positions of Cu ions in the lattice and the corresponding polarizations as per the quadruple well. The trajectory of Cu atoms that is consistent with the discussed polarization sequence is shown in Fig. 3(c). The arrows on the right side of Fig. 3(c) depict the polarization sequence, which is consistent with the quadruple well, where the length of the arrow indicates the low- or high-polarization phase. Other Cu trajectories, ranging from a single layer to three layers and two vdW gaps which account for other polarization sequences in the Sankey

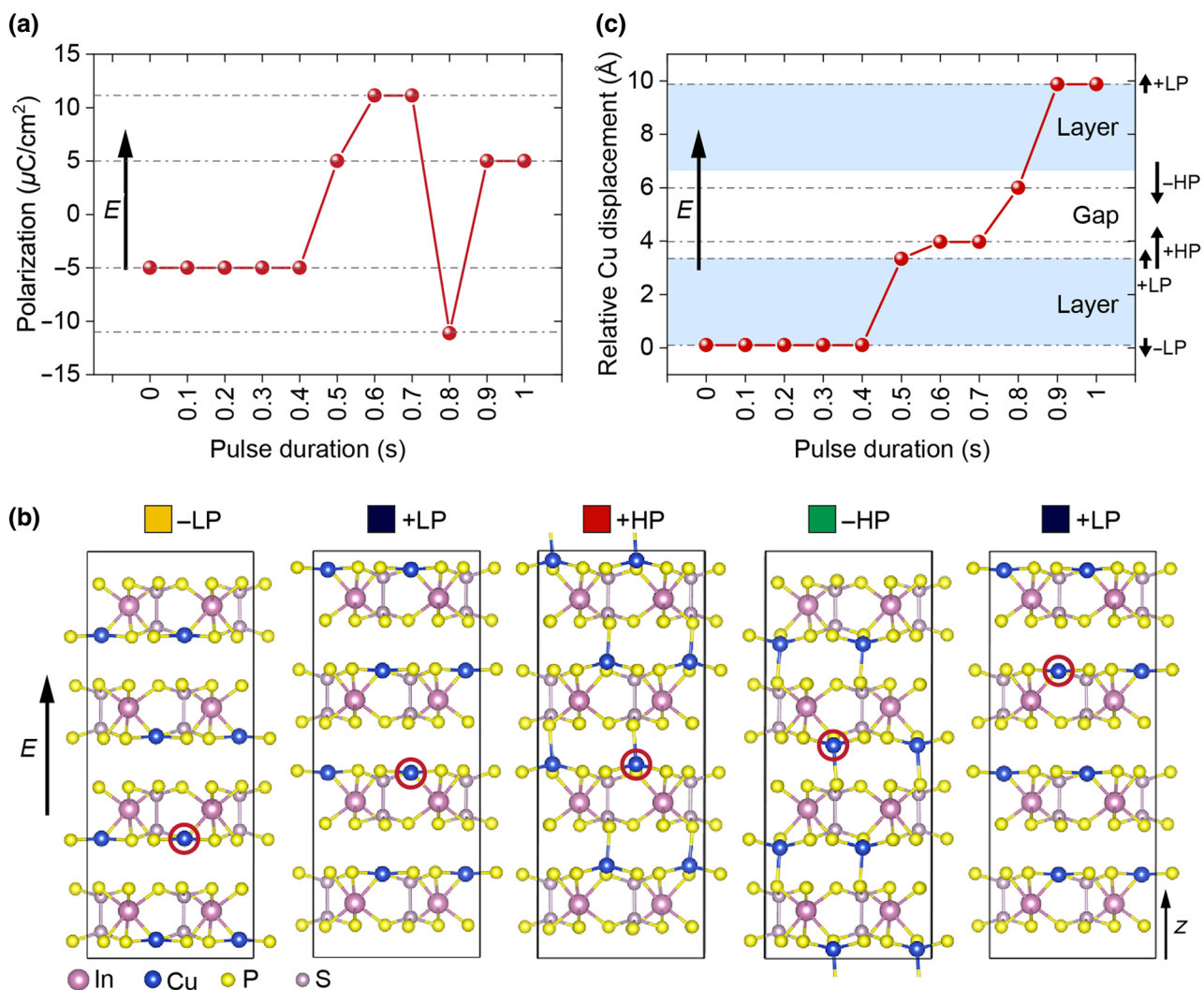


FIG. 3. Trajectory of Cu during switching experiment. (a) Polarization as a function of pulse duration for the path outlined by the dashed line in Fig. 2. Direction of the applied electric field is indicated by black arrow. (b) Structural phases involved in the switching pathway shown in (a). The red circle indicates one specific atom in the structure, which can be moved by the applied electric field. Direction of the applied electric field and individual polarization states are indicated by black arrows. (c) Relative Cu displacement as function of pulse duration for the path outlined in (a).

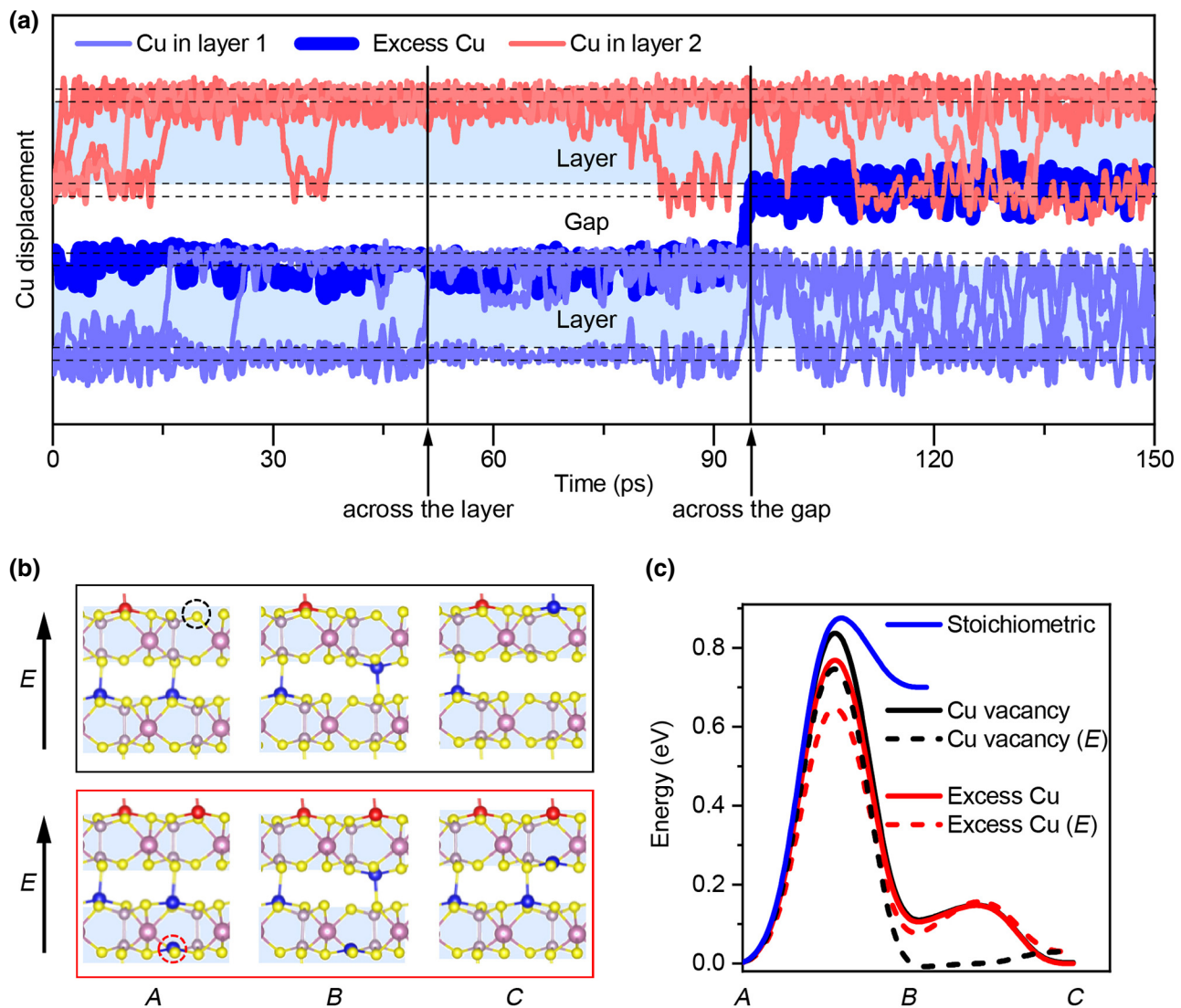


FIG. 4. Simulation of ferroelectric switching in  $\text{CuInP}_2\text{S}_6$ . (a) Trajectory of Cu ions in two individual layers with excess Cu under application of an external electric field. Excess Cu is marked by dark blue. Two arrows indicate times when all Cu move across the layer and one Cu atom moves across the vdW gap, respectively. (b) Configurations tracking Cu migration in the presence of a vacancy identified by a dashed black circle, and lower panel (outlined in red) in the presence of excess Cu identified by a dashed red circle: initial +HP state (a), intermediate -HP state (b), and final +HP state (c). (c) Energy barriers for a Cu atom migrating from the +HP state of one layer to the -HP state of the adjacent layer corresponding to (a). Solid black curve and solid red curve are the energy profiles with a vacancy and excess Cu, respectively. When an external electric field ( $-1.0 \text{ V/\AA}$ ) is applied along the  $z$  direction, energy profiles are shown as dashed curves. Solid blue curve is the pathway for a Cu atom jumping across the vdW gap in stoichiometric four-layer  $\text{CuInP}_2\text{S}_6$ .

diagram, are discussed in detail in the Supplemental Material (Fig. S2) [44].

Next, we explore if an alternative explanation of the experimental data is possible, in terms of partial polarization switching, i.e., low values of  $d$  do not depict the HP polarization state as assigned in Fig. 1(b). The  $d$  values of the individual switching pathway shown in Fig. 3 are depicted in the Supplemental Material (Fig. S3) [44]. After the measurement of high positive and high negative  $d$

values, we observe low  $d$  values, which is inconsistent with the idea of partial switching.

### C. Simulation of copper paths

To further understand the atomic-scale mechanisms of the complex polarization transitions of Fig. 3 and make a connection to ionic conduction, we perform QMD simulations in supercells containing four  $\text{CuInP}_2\text{S}_6$

layers plus vacuum under an applied electric field of  $-1.0 \text{ V/\AA}$  at 200 K. We adopt stoichiometric supercells and supercells that contain a Cu vacancy or an extra Cu atom because such point defects are known to facilitate long-range migration [45]. Figure 4(a) shows the  $z$  trajectories of Cu atoms in supercells containing an extra Cu atom. At first, the Cu atoms oscillate randomly between the  $-HP$  and  $-LP$  energy minima (the bottom of the layers), except for the extra Cu atom (marked in blue), which stays at the top of the layer. After 51 ps, all four Cu atoms in the “red” layer switch from the bottom of the layer to the top, while in the “blue” layer, which contains an excess Cu at the top of the layer, one Cu is left at the bottom of the layer. In this process, the switching pathway is from negative to positive polarization states through the  $\text{CuInP}_2\text{S}_6$  layer, following the direction of the external electric field. Once the events described above are observed, indicating normal ferroelectric switching within individual layers, the temperature is increased to 500 K (above the Curie temperature) to speed up the simulation and observe interlayer jumps, which entail a higher energy barrier. At 95 ps, the excess Cu atom moves across the vdW gap and into the bottom of the adjacent layer. In this process, the switching pathway is from a positive to negative polarization state, which is consistent with the experimentally observed alignment against the external electric field.

The QMD simulations demonstrate the key feature that individual Cu atoms make their jumps between equilibrium sites within layers and across vdW gaps at different times, i.e., at picosecond timescales. We further examine the static energy barriers that individual Cu atoms face in crossing the vdW gap in stoichiometric  $\text{CuInP}_2\text{S}_6$  and when the initial layer contains an extra Cu or the final layer contains a vacancy, without and with an electric field. Figure 4(b) shows individual Cu jumps across the vdW gap in the presence of a Cu vacancy (top) and an excess Cu atom (bottom), as the structure transitions through  $A-C$  with or without an applied electric field. The calculated energy barriers for these transitions are shown in Fig. 4(c). The energy barriers in Fig. 4(c) range from 0.6 to 0.8 eV for the different scenarios, which matches experimentally observed activation barriers in the range of 0.63–1.09 eV obtained through dielectric measurements [1,18,46] and Cu particle formation [17]. We note that defects, especially extra Cu atoms, and the electric field lower the activation barrier. These energy barriers for individual Cu atom jumps are related to, but are not necessarily identical to, those appearing in the quadruple-well potential, because the latter is calculated by moving entire Cu sheets simultaneously, which can be viewed as an average on mesoscopic timescales. We finally note that the energy cost for Frenkel-pair thermal creation is relatively small, about 0.7 eV, whereby there is a plentiful supply of Cu vacancies and interstitials to facilitate interlayer jumps. On

the other hand, the layers remain essentially stoichiometric over macroscopic timescales.

In  $\text{CuInP}_2\text{S}_6$ , the presence of long-range ionic conduction of Cu ions is further supported by experimental observations, which show measurable current during the application of switching pulses, when the pulse duration is longer than 0.5 s. In addition, we have previously shown that Cu ions can be extracted from the crystal lattice by applying negative voltages to the PFM tip, which is used to extract the activation energy for ionic transport [17,18]. In the case of the capacitor used here, it is also observed that, after application of long negative  $V_{dc}$  pulses of several seconds (Fig. S4 within the Supplemental Material [44]), the edges of the capacitor structures start to show topographic features similar to those obtained on a bare surface at higher temperature [17]. This observation further corroborates that we are able to move Cu over length scales larger than the unit cell, even at room temperature.

#### IV. CONCLUSIONS

We demonstrate a mechanism that allows transitioning between polarization states via field-driven motion of ions through the crystal. The effect is demonstrated in layered  $\text{CuInP}_2\text{S}_6$ , which is ferroelectric at room temperature and a good ion conductor involving the same ionic species (Cu). The process of Cu motion across the vdW gap results in alignment of the polarization vector against the applied electric field and is fundamentally different from normal ferroelectric switching, i.e., permanent-dipole reorientation, as well as prior reports of so-called anomalous switching, such as back-switching events produced by image charges [7,47–49] and switching via surface chemistry [50] and stress [51–54]. The mechanism demonstrated in this paper enables transitioning between all polarization states with a unidirectional electric field, providing exciting opportunities for ferroelectric information technology beyond binary limitations, for example, in ferroelectric memories [55–58] or solid-state synapses [59]. Moreover, by controlled switching from low- to high-polarization states, not only electromechanical but also other material properties are expected to change, unlocking further potential applications in optics and electronics. For many practical applications, a faster timescale of the described process is required. Faster switching times can be achieved by increasing the ion conductivity, which can be tuned by sample composition, sample thickness, electrode size, and electric field gradients, and is subject to future studies. A fascinating fundamental question is the structure of propagating domain fronts, coupled with ionic motion and the degree to which the two processes synchronize in space and time.

## ACKNOWLEDGMENTS

The experimental work as well as data analysis and interpretation are supported by the U.S. Department of Energy (DOE), Office of Science, Basic Energy Sciences, Materials Science, and Engineering Division. The experiments are conducted at the Center for Nanophase Materials Sciences, which is a DOE Office of Science User Facility. Theoretical work at Vanderbilt University is supported by the U.S. Department of Energy, Office of Science, Division of Materials Science and Engineering Grant No. DE-FG02-09ER46554 and by the McMinn Endowment. The work at Purdue University was supported in part by a NSF/AFOSR EFRI 2DARE programme and in part by an ARO programme.

- [1] S. Zhou, L. You, A. Chaturvedi, S. A. Morris, J. S. Herrin, N. Zhang, A. Abdelsamie, Y. Hu, J. Chen, Y. Zhou, S. Dong, and J. Wang, Anomalous polarization switching and permanent retention in a ferroelectric ionic conductor, *Mater. Horiz.* **7**, 263 (2020).
- [2] Q. Jiang, M. N. Womersley, P. A. Thomas, J. P. Rourke, K. B. Hutton, and R. C. C. Ward, Ferroelectric, conductive, and dielectric properties of  $\text{KTiOPO}_4$  at low temperature, *Phys. Rev. B* **66**, 094102 (2002).
- [3] J. F. Scott, F. Habbal, and J. A. Zvirgzds, Ferroelectric phase transition in the superionic conductor  $\text{Ag}_{26}\text{I}_{18}\text{W}_4\text{O}_{16}$ , *J. Chem. Phys.* **72**, 2760 (1980).
- [4] Ch. Muller, J.-C. Valmalette, J.-L. Soubeyroux, F. Bouree, and J.-R. Gavarrı, Structural disorder and ionic conductivity in  $\text{LiVO}_3$ : A neutron powder diffraction study from 340 to 890 K, *J. Solid State Chem.* **156**, 379 (2001).
- [5] W. S. Tang, M. Dimitrievska, V. Stavila, W. Zhou, H. Wu, A. A. Talin, and T. J. Udovic, Order–disorder transitions and superionic conductivity in the sodium nido-undeca(carba)borates, *Chem. Mater.* **29**, 10496 (2017).
- [6] A. V. Ievlev, A. N. Morozovska, E. A. Eliseev, V. Y. Shur, and S. V. Kalinin, Ionic field effect and memristive phenomena in single-point ferroelectric domain switching, *Nat. Commun.* **5**, 4545 (2014).
- [7] S. M. Neumayer, A. V. Ievlev, L. Collins, R. Vasudevan, M. A. Baghban, O. Ovchinnikova, S. Jesse, K. Gallo, B. J. Rodriguez, and S. V. Kalinin, Surface chemistry controls anomalous ferroelectric behavior in lithium niobate, *ACS Appl. Mater. Interfaces* **10**, 29153 (2018).
- [8] E. A. Eliseev, A. N. Morozovska, G. S. Svechnikov, E. L. Rumyantsev, E. I. Shishkin, V. Y. Shur, and S. V. Kalinin, Screening and retardation effects on  $180^\circ$ -domain wall motion in ferroelectrics: Wall velocity and nonlinear dynamics due to polarization- screening charge interactions, *Phys. Rev. B - Condens. Matter Mater. Phys.* **78**, 1 (2008).
- [9] C. Long, W. Ren, Y. Li, L. Liu, Y. Xia, and H. Fan, High oxide ion conductivity in layer-structured  $\text{Bi}_4\text{Ti}_3\text{O}_{12}$ -based ferroelectric ceramics, *J. Mater. Chem. C* **7**, 8825 (2019).
- [10] F. Habbal, J. A. Zvirgzds, and J. F. Scott, Raman spectroscopy of structural phase transitions in  $\text{Ag}_{26}\text{I}_{18}\text{W}_4\text{O}_{16}$ , *J. Chem. Phys.* **69**, 4984 (1978).
- [11] A. I. Baranov, V. P. Khiznichenko, and L. A. Shuvalov, High temperature phase transitions and proton conductivity in some kdp-family crystals, *Ferroelectrics* **100**, 135 (1989).
- [12] J. F. Scott, A comparison of Ag- and proton-conducting ferroelectrics, *Solid State Ion.* **125**, 141 (1999).
- [13] V. Maisonneuve, V. Cajipe, A. Simon, R. Von Der Muhll, and J. Ravez, Ferrielectric ordering in lamellar  $\text{CuInP}_2\text{S}_6$ , *Phys. Rev. B* **56**, 10860 (1997).
- [14] A. Belianinov, Q. He, A. Dziaugys, P. Maksymovych, E. Eliseev, A. Borisevich, A. Morozovska, J. Banys, Y. Vysochanskii, and S. V. Kalinin,  $\text{CuInP}_2\text{S}_6$  room temperature layered ferroelectric, *Nano Lett.* **15**, 3808 (2015).
- [15] M. Chyasnovichus, M. A. Susner, A. V. Ievlev, E. A. Eliseev, S. V. Kalinin, N. Balke, A. N. Morozovska, M. A. McGuire, and P. Maksymovych, Size-effect in layered ferrielectric  $\text{CuInP}_2\text{S}_6$ , *Appl. Phys. Lett.* **109**, 172901 (2016).
- [16] F. Liu, L. You, K. L. Seyler, X. Li, P. Yu, J. Lin, X. Wang, J. Zhou, H. Wang, H. He, S. T. Pantelides, W. Zhou, P. Sharma, X. Xu, P. M. Ajayan, J. Wang, and Z. Liu, Room-temperature ferroelectricity in  $\text{CuInP}_2\text{S}_6$  ultrathin flakes, *Nat. Commun.* **7**, 12357 (2016).
- [17] N. Balke, S. M. Neumayer, J. A. Brehm, M. A. Susner, B. J. Rodriguez, S. Jesse, S. V. Kalinin, S. T. Pantelides, M. A. McGuire, and P. Maksymovych, Locally controlled Cu-ion transport in layered ferroelectric  $\text{CuInP}_2\text{S}_6$ , *ACS Appl. Mater. Interfaces* **10**, 27188 (2018).
- [18] V. Maisonneuve, J. M. Reau, M. Dong, V. B. Cajipe, C. Payen, and J. Ravez, Ionic conductivity in ferroic  $\text{CuInP}_2\text{S}_6$  and  $\text{CuCrP}_2\text{S}_6$ , *Ferroelectrics* **196**, 257 (1997).
- [19] M. A. Susner, M. Chyasnovichus, M. A. McGuire, P. Ganesh, and P. Maksymovych, Metal thio- and selenophosphates as multifunctional van der Waals layered materials, *Adv. Mater.* **9**, 1602852 (2017).
- [20] L. You, Y. Zhang, S. Zhou, A. Chaturvedi, S. A. Morris, F. Liu, L. Chang, D. Ichinose, H. Funakubo, W. Hu, T. Wu, Z. Liu, S. Dong, and J. Wang, Origin of giant negative piezoelectricity in a layered van der waals ferroelectric, *Sci. Adv.* **5**, eaav3780 (2019).
- [21] J. A. Brehm, S. M. Neumayer, L. Tao, A. O'Hara, M. Chyasnovichus, M. A. Susner, M. A. McGuire, S. V. Kalinin, S. Jesse, P. Ganesh, S. T. Pantelides, P. Maksymovych, and N. Balke, Tunable quadruple-well ferroelectric van-der-Waals crystals, *Nat. Mater.* **19**, 43 (2020).
- [22] S. M. Neumayer, E. A. Eliseev, M. A. Susner, A. Tselev, B. J. Rodriguez, J. A. Brehm, S. T. Pantelides, G. Panchapakesan, S. Jesse, S. V. Kalinin, M. A. McGuire, A. N. Morozovska, P. Maksymovych, and N. Balke, Giant negative electrostriction and dielectric tunability in a van der Waals layered ferroelectric, *Phys. Rev. Mater.* **3**, 024401 (2019).
- [23] M. Si, A. K. Saha, P.-Y. Liao, S. Gao, S. M. Neumayer, J. Jian, J. Qin, N. Balke, H. Wang, P. Maksymovych, W. Wu, S. K. Gupta, and P. D. Ye, Room temperature electrocaloric effect in 2D ferroelectric  $\text{CuInP}_2\text{S}_6$  for nano-refrigerator, *ACS Nano* **13**, 8760 (2019).

- [24] G. Kresse and J. Furthmüller, Efficient iterative schemes for ab initio total-energy calculations using a plane-wave basis set, *Phys. Rev. B* **54**, 11169 (1996).
- [25] P. E. Blochl, Projector augmented wave method, *Phys. Rev. B* **50**, 17953 (1994).
- [26] G. Kresse and D. Joubert, From ultrasoft pseudopotentials to the projector augmented-wave method, *Phys. Rev. B* **59**, 1758 (1999).
- [27] J. P. Perdew, K. Burke, and M. Ernzerhof, Generalized Gradient Approximation Made Simple, *Phys. Rev. Lett.* **77**, 3865 (1996).
- [28] S. Grimme, S. Ehrlich, and L. Goerigk, Effect of the damping function in dispersion corrected density functional theory, *J. Comput. Chem.* **32**, 1456 (2011).
- [29] A. D. Becke and E. R. Johnson, A density-functional model of the dispersion interaction, *J. Chem. Phys.* **123**, 154101 (2005).
- [30] G. Henkelman, B. P. Uberuaga, and H. Jonsson, A climbing image nudged elastic band method for finding saddle points and minimum energy paths, *J. Chem. Phys.* **113**, 9901 (2000).
- [31] G. Mills, H. Jonsson, and G. K. Schenter, Reversible work transition-state theory - application to dissociative adsorption of hydrogen, *Surf. Sci.* **324**, 305 (1995).
- [32] J. Neugebauer and M. Scheffler, Adsorbate-substrate and adsorbate-adsorbate interactions of Na and K adlayers on Al(111), *Phys. Rev. B* **46**, 16067 (1992).
- [33] G. Makov and M. C. Payne, Periodic boundary-conditions in ab-initio calculations, *Phys. Rev. B* **51**, 4014 (1995).
- [34] G. Kresse and J. Hafner, Ab-initio molecular-dynamics for open-shell transition-metals, *Phys. Rev. B* **48**, 13115 (1993).
- [35] G. Kresse and J. Hafner, Ab-initio molecular-dynamics simulation of the liquid-metal amorphous-semiconductor transition in germanium, *Phys. Rev. B* **49**, 14251 (1994).
- [36] I. Urbanavičiūtė, T. D. Cornelissen, X. Meng, R. P. Sijbesma, and M. Kemerink, Physical reality of the Preisach model for organic ferroelectrics, *Nat. Commun.* **9**, 4409 (2018).
- [37] D. A. Gilbert, G. T. Zimanyi, R. K. Dumas, M. Winklhofer, A. Gomez, N. Eibagi, J. L. Vicent, and K. Liu, Quantitative decoding of interactions in tunable nanomagnet arrays using first order reversal curves, *Sci. Rep.* **4**, 4204 (2015).
- [38] A. Stancu, D. Ricinchi, L. Mitoseriu, P. Postolache, and M. Okuyama, First-order reversal curves diagrams for the characterization of ferroelectric switching, *Appl. Phys. Lett.* **83**, 3767 (2003).
- [39] A. Stancu, C. Pike, L. Stoleriu, P. Postolache, and D. Cimpoesu, Micromagnetic and preisach analysis of the first order reversal curves (FORC) diagram, *J. Appl. Phys.* **93**, 6620 (2003).
- [40] Y. Kim, A. Kumar, O. Ovchinnikov, S. Jesse, H. Han, D. Pantel, I. Vrejoiu, W. Lee, D. Hesse, M. Alexe, and S. V. Kalinin, First-order reversal curve probing of spatially resolved polarization switching dynamics in ferroelectric nanocapacitors, *ACS Nano* **6**, 491 (2012).
- [41] A. Gruverman, B. J. Rodriguez, A. I. Kingon, R. J. Nemanich, J. S. Cross, and M. Tsukada, Spatial inhomogeneity of imprint and switching behavior in ferroelectric capacitors, *Appl. Phys. Lett.* **82**, 3071 (2003).
- [42] A. Gruverman, D. Wu, and J. F. Scott, Piezoresponse Force Microscopy Studies of Switching Behavior of Ferroelectric Capacitors on a 100-ns Time Scale, *Phys. Rev. Lett.* **100**, 097601 (2008).
- [43] N. Setter, D. Damjanovic, L. Eng, G. Fox, S. Gevorgian, S. Hong, A. Kingon, H. Kohlstedt, N. Y. Park, G. B. Stephenson, I. Stolitchnov, A. K. TagansteV, D. V. Taylor, T. Yamada, and S. Streiffier, Ferroelectric thin films: Review of materials, properties, and applications, *J. Appl. Phys.* **100**, 051606 (2006).
- [44] See the Supplemental Material at <http://link.aps.org/supplemental/10.1103/PhysRevApplied.13.064063> for detailed transition analysis, further Cu trajectories, assignment of piezoelectric constants to polarization states, and electrode topography after a long voltage pulse.
- [45] R. Car, P. J. Kelly, A. Oshiyama, and S. T. Pantelides, Microscopic theory of atomic diffusion mechanisms in silico, *Proc. 4th Gen. Conf. Condens. Matter Div. EPS* **127**, 401 (1984).
- [46] J. Banys, J. Macutkevicius, V. Samulionis, A. Brilingas, and Yu. Vysochanskii, Dielectric and ultrasonic investigation of phase transition in cuinp2s6 crystals, *Phase Transit.* **77**, 345 (2004).
- [47] V. Ya. Shur, Domain nanotechnology in ferroelectrics: Nano-domain engineering in lithium niobate crystals, *Ferroelectrics* **373**, 1 (2008).
- [48] A. Ievlev and S. V. Kalinin, Data encoding based on the shape of the ferroelectric domains produced by using a scanning probe microscopy tip, *Nanoscale* **7**, 11040 (2015).
- [49] A. V. Ievlev, D. O. Alikin, A. N. Morozovska, O. V. Varenyk, E. A. Eliseev, A. L. Kholkin, X. V. Y. Shur, and S. V. Kalinin, Symmetry breaking and electrical frustration during tip-induced polarization switching in the nonpolar cut of lithium niobate single crystals, *ACS Nano* **9**, 769 (2015).
- [50] Y. Tian, L. Wei, Q. Zhang, H. Huang, Y. Zhang, H. Zhou, F. Ma, L. Gu, S. Meng, L.-Q. Chen, C.-W. Nan, and J. Zhang, Water printing of ferroelectric polarization, *Nat. Commun.* **9**, 3809 (2018).
- [51] H. Lu, C.-W. Bark, D. Esque de los Ojos, J. Alcalá, C. B. Eom, G. Catalan, and A. Gruverman, Mechanical writing of ferroelectric polarization, *Science* **336**, 59 (2012).
- [52] A. Alsubaie, P. Sharma, G. Liu, V. Nagarajan, and J. Seidel, Mechanical stress-induced switching kinetics of ferroelectric thin films at the nanoscale, *Nanotechnology* **28**, 075709 (2017).
- [53] J. Rouquette, J. Haines, V. Bornand, M. Pintard, Ph. Papet, W. G. Marshall, and S. Hull, Pressure-induced rotation of spontaneous polarization in monoclinic and triclinic  $\text{PbZr}_{0.52}\text{Ti}_{0.48}\text{O}_3$ , *Phys. Rev. B* **71**, 024112 (2005).
- [54] Y. Cao, A. Morozovska, and S. V. Kalinin, Pressure-induced switching in ferroelectrics: Phase-field modeling, electrochemistry, flexoelectric effect, and bulk vacancy dynamics, *Phys. Rev. B* **96**, 184109 (2017).
- [55] J. F. Scott, Applications of modern ferroelectrics, *Science* **315**, 954 (2007).
- [56] J. F. Scott, C. A. Paz de Araujo, Ferroelectric memories, *Science* **246**, 1400 (1989).

- [57] J. Hoffman, X. Pan, J. W. Reiner, F. J. Walker, J. P. Han, C. H. Ahn, and T. P. Ma, Ferroelectric field effect transistors for memory applications, *Adv. Mater.* **22**, 2957 (2010).
- [58] M. Dawber, K. M. Rabe, and J. F. Scott, Physics of thin-film ferroelectric oxides, *Rev. Mod. Phys.* **77**, 1083 (2005).
- [59] S. Boyn, J. Grollier, G. Lecerf, B. Xu, N. Locatelli, S. Fusil, S. Girod, C. Carrétéro, K. Garcia, S. Xavier, J. Tomas, L. Bellaiche, M. Bibes, A. Barthélémy, S. Saïghi, and V. Garcia, Learning through ferroelectric domain dynamics in solid-state synapses, *Nat. Commun.* **8**, 14736 (2017).